Journal of Biomolecular NMR **28:** 137–155, 2004.
KLUWER/ESCOM

Solution structure and backbone dynamics of the pleckstrin homology domain of the human protein kinase B (PKB/Akt). Interaction with inositol phosphates

Daniel Auguin[a], Philippe Barthe[a], Marie-Thérèse Augé-Sénégas[a], Marc-Henri Stern[b], Masayuki Noguchi[c] & Christian Roumestand[a,*]

[a]*Centre de Biochimie Structurale, UMR 5048 CNRS/UM1 – UMR 554 INSERM/UM1, Faculté de Pharmacie, BP14491, 15 Avenue Charles Flahault, 34093 Montpellier Cedex 5, France;* [b]*Unité INSERM U509, Institut Curie, Section de Recherche, 26 rue d'Ulm, F75248 Paris Cedex 5, France;* [c]*Division of Cancer Biology, Institute for Genetic Medicine, Hokkaido University, N15 W7, Kita-ku, Sapporo 060-0815, Japan*

Received 19 June 2003; Accepted 3 September 2003

Key words: Akt, apoptosis, inositol phosphate, NMR, PKB, pleckstrin homology domain, proliferation, solution structure

Abstract

The programmed cell death occurs as part of normal mammalian development. The induction of developmental cell death is a highly regulated process and can be suppressed by a variety of extracellular stimuli. Recently, the ability of trophic factors to promote survival have been attributed, at least in part, to the phosphatidylinositide 3′-OH kinase (PI3K)/Protein Kinase B (PKB, also named Akt) cascade. Several targets of the PI3K/PKB signaling pathway have been identified that may underlie the ability of this regulatory cascade to promote cell survival. PKB possesses a N-terminal Pleckstrin Homology (PH) domain that binds specifically and with high affinity to PtIns(3,4,5)P_3 and PtIns(3,4)P_2, the PI3K second messengers. PKB is then recruited to the plasma membrane by virtue of its interaction with 3′-OH phosphatidylinositides and activated. Recent evidence indicates that PKB is active in various types of human cancer; constitutive PKB signaling activation is believed to promote proliferation and increased cell survival, thereby contributing to cancer progression. Thus, it has been shown that induction of PKB activity is augmented by the TCL1/MTCP1 oncoproteins through a physical association requiring the PKB PH domain. Here we present the three-dimensional solution structure of the PH domain of the human protein PKB (isoform β). PKBβ-PH is an electrostatically polarized molecule that adopts the same fold and topology as other PH-domains, consisting of a β-sandwich of seven strands capped on one top by an α-helix. The opposite face presents three variable loops that appear poorly defined in the NMR structure. Measurements of ^{15}N spin relaxation times and heteronuclear ^{15}N{^{1}H}NOEs showed that this poor definition is due to intrinsic flexibility, involving complex motions on different time scales. Chemical shift mapping studies correctly defined the binding site of Ins(1,3,4,5)P_4 (the head group of PtIns(3,4,5)P_3), as was previously proposed from a crystallographic study. More interestingly, these studies allowed us to define a putative alternative low-affinity binding site for Ins(1,4,5)P_3. The binding of this sugar to PKBβ-PH might also involve non-specific association that could explain the stabilization of the protein in solution in the presence of Ins(1,4,5)P_3.

*To whom correspondence should be addressed.
E-mail: christian.roumestand@cbs.cnrs.fr

Abbreviations: PH – pleckstrin homology domain; PKBβ – Protein kinase B (isoform β); PtIns(3,4,5)P_3 – Phosphatidylinositol-3,4,5-tris phosphate; PtIns(3,4)P_2 – Phosphatidylinositol-3,4-bis phosphate; Ins(1,3,4,5)P_4 or IP_4 – inositol-1,3,4,5-tetrakis phosphate; Ins(1,4,5)P_3 or IP_3 – inositol-1,4,5-tris phosphate; DTNB – 5,5′-dithiobis(2-nitrobenzoic acid); EDTA – Ethylenediamine tetracetic acid; IPTG – Isopropyl-thio-β-D-galactopyranoside; DSS – 2,2-dimethyl-2-silapentane-5-sulfonate sodium salt; 2(3)D – two(three)-dimensional; NOE – nuclear Overhauser enhancement; $^{15}N\{^1H\}$ NOE – heteronuclear ^{15}N nuclear Overhauser enhancement; $R_N(N_z)$ (R_1) – heteronuclear ^{15}N longitudinal relaxation rate; $R_N(N_{xy})$ (R_2) – heteronuclear ^{15}N transverse relaxation rate; $R_N(H_z \rightarrow N_z)$ (σ) – cross-relaxation rate between ^{15}N and its attached amide proton; r.m.s.d. – root mean square deviation; T-PLL – T-cell Prolymphocytic Leukemia.

Introduction

The genes of PKB were first identified as human homologues of the viral oncogene of v-Akt, previously known to cause a form of leukemia in mice (Staal, 1987), hence the frequent use of the name Akt. Subsequently, three independent studies revealed that v-Akt and its mammalian homologues encoded a protein kinase with some similarities to protein kinase C (PKC) and Protein kinase A (PKA) (Bellacosa et al., 1991; Coffer and Woodgett, 1991; Jones et al., 1991a). Its relatedness to PKA and PKC led to it being named PKB by the authors of one of these studies. There are three highly homologous PKB (70–80% homology at the amino-acid level) isoforms in mammals (PKBα, PKBβ and PKBγ, also known as Akt1, Akt2 and Akt3) that are expressed ubiquitously, although PKBγ has a more restricted tissue distribution. PKB is a 57–60 kDa member of the AGC super-family of serine/threonine protein kinases that is activated by cytokines, antigen receptors, the co-stimulator CD28 and chemokines in lymphocytes. As a result, PKB has emerged as a crucial regulator of widely divergent cellular processes including apoptosis, proliferation, differentiation and metabolism (for reviews see Datta and Greenberg, 1999; Nicholson and Anderson, 2002; Cantrell, 2002). Activation of PKB signaling has now been documented as a frequent occurrence in several human cancers and this enzyme appears to play an important role in their progression. In response to growth factors and other extra cellular stimuli, PKB is activated in a pathway induced by the lipid products of the phosphoinositide 3′-kinase (PI3K), which phosphorylate the 3-OH position of the inositol core of inositol phospholipids (PtdIns). PKB has a hydrophobic C-terminal regulatory motif, a catalytic domain – that shows a high degree of similarity to those found in PKA and PKC (Jones et al., 1991b, Andjelkovic et al., 1995; Yang et al., 2002) – and a N-terminal pleckstrin homology (PH) domain. The PH domain family, first identified in 1993 as a 100–120-residue module that occurs twice in pleckstrin (Haslam, 1993), appears to be a very large family of homologous protein domains of moderate to low sequence similarity (reviewed in Lemmon and Ferguson, 1998; Rebecchi and Scarlata, 1998). From inspection of the human genome, 252 PH domains have been detected in protein sequences (Lander et al., 2001). The PH domain is believed to play a role in intracellular signal transduction, and the functional role of the PH domain has been characterized for several systems. In these cases, the PH domain binds with high affinity and specificity to a phosphoinositide. The PH domain of PKB binds with high affinity and specificity the lipid second messengers PtdIns(3,4)P_2 and PtdIns(3,4,5)P_3, the products of agonist-stimulated PI3K. PKB activation is initiated by the binding of PtdIns(3,4,5)P_3 to the PH domain of the enzyme that recruits the kinase to the plasma membrane where it is phosphorylated on Thr^{308}, in the catalytic domain, and on Ser^{473}, in the C-terminal hydrophobic motif (Alessi et al., 1996). PKB may also be phosphorylated on Ser^{124} and Thr^{450} but neither of these sites appears to regulate PKB activity and their phosphorylation does not change following cell stimulation (Alessi et al., 1996).

Recently, it has been shown that induction of PKB serine/threonine kinase activity is augmented by the TCL1/MTCP1 oncoproteins through a physical association requiring the PKB pleckstrin homology domain (Laine et al., 2000; Künstle et al., 2002; French et al., 2002), mediating the formation of oligomeric TCL1/MTCP1-PKB high molecular weight protein complexes *in vivo* (Laine et al., 2000; Künstle et al., 2002). Within these complexes, PKB is preferentially phosphorylated and activated. The *MTCP1* gene, located in the Xq28 chromosomal region, was the first gene to be identified in T-cell prolymphocytic leukemia (T-PLL) presenting a mature phenotype (Stern et al., 1993). It is involved in the translocation t(X;14)(q28;q11), a translocation recurrently associ-

ated with this type of T-cell proliferations. It codes for a 107 residues (13 kDa) protein known as $p13^{MTCP1}$ (Madani et al., 1996), the expression of which is restricted to mature T-cell proliferations with t(X;14) translocations (Madani et al., 1996). This protein shows high sequence homology (40% identity, 61% similarity) with $p14^{TCL1}$ (Fu et al., 1994), the product of the 14q32.1 oncogene TCL1, and with $p14^{TCL1b}$ (28% identity, 48% similarity), the product of the closely related TCL-1b oncogene (Pekarsky, 1999). In human diseases, in addition to T-PLL, TCL1 is overexpressed in a number of malignant B-cell proliferations. We have previously solved the crystal structure of $p14^{TCL1}$ (Hoh et al., 1998) and the solution structure of $p13^{MTCP1}$ (Yang et al., 1998; Guignard et al., 2000): They adopt a similar β-barrel fold with a new topology, the essential difference being that $p14^{TCL1b}$ forms a dimer in the crystal as well as in solution, whereas $p13^{MTCP1}$ is monomeric. More recently, the X-Ray structure of the PKBα PH domain (PKBα-PH) in complex with Inositol-4-Phosphate ($Ins(1,3,4,5)P_4$: the head-group of $PtdIns(3,4,5)P_3$) has been determined to 1.4 Å resolution (Thomas et al., 2002), providing detailed information on the interaction of the PH-domain with $PtdIns(3,4,5)P_3$. In the present paper, we report the solution structure of PKBβ-PH (73% homology) in the presence of $Ins(1,4,5)P_3$. We complemented the structural study by an analysis of the backbone dynamics using experimental ^{15}N relaxation parameters measured on the NH vectors. These results are of paramount importance to gain information on the interaction between PKB-PH and the TCL1/MTCP1 proto-oncogenes *via* chemical shift mapping studies, and a first step toward the structure of the PKBβ-PH/$p13^{MTCP1}$ or PKBβ-PH/$p14^{TCL1}$ complexes.

Materials and methods

Protein preparation

The production of the recombinant PKBβ/Akt2 Pleckstrin Homology domain will be published in detail elsewhere. Briefly, PKBβ PH domain was amplified by PCR from human EBV transformed B cell cDNA library. The cDNA encoding the 111 N-terminal residues of human PKBβ/Akt2 – corresponding to the Pleckstrin Homology domain – was sub-cloned into the *Eco*RI *Bam*HI sites of the pGEX2T plasmid. Uniformly labeled ^{15}N and or ^{13}C recombinant protein was obtained from over-expression in *E. coli* BL21 grown in minimal medium containing $^{15}NH_4Cl$ as the sole nitrogen source, and either ^{13}C- or unlabeled glucose. The GST-fusion protein was purified using affinity chromatography on glutathione-sepharose beads (Pharmacia), then cleaved overnight by adding thrombin to the beads in a low salt buffer. Eluted protein was further purified using size exclusion chromatography with an HR100 column (Pharmacia). The different preparations yield about 15 mg of each protein (unlabeled, ^{15}N-labeled, and ^{13}C,^{15}N-labeled) that were conditioned at a concentration of 0.4 mM in the buffer used for NMR spectroscopy (10 mM Tris/H_2O (pH 7.4), 300 mM NaCl, 0.1 mM benzamidine, 0.1 mM EDTA).

Thiol titration

The titration of thiol groups in the protein was done according to Ellman's method (Riddles et al., 1983) by incubating (5 mn) an aliquot of 10 µl from the NMR sample in a freshly prepared solution of DTNB. No absorption was measured at 412 nm, indicating no release of TNB in solution due to the reaction of DTNB with a free SH group. The same test was performed in the presence of 6 M of GuHCl, in order to unfold the protein, thus facilitating the access of DTNB to eventually buried SH groups: Again, no absorption was detected. As a result, the two cystinyl residues present in the protein sequence are involved in a disulfide bond.

NMR measurements

NMR spectra were recorded on 0.25–0.3 ml (Shigemi tubes pre-coated with a silicon solution (Sigma)) samples of 0.4 mM, ^{15}N or ^{15}N,^{13}C labeled PKBβ-PH dissolved in the conditioning buffer (with 5–10% ^2H_2O for the lock) and in the presence of 4 mM $Ins(1,4,5)P_3$. Some spectra were also collected on samples prepared in ^2H_2O containing buffer. NMR experiments were carried out at 13 °C on Bruker AVANCE 500 and 600 spectrometers equipped with 5 mm *z*-shielded gradient ^1H-^{13}C-^{15}N triple resonance conventional (600 MHz) or cryogenic (500 MHz) probes. ^1H chemical shifts were directly referenced to the resonance of 2,2-dimethyl-2-silapentane-5-sulfonate sodium salt (DSS), while ^{13}C and ^{15}N chemical shifts were indirectly referenced with the absolute frequency ratios $\Xi(^{13}C/^1H) = 0.251449530$ and $\Xi(^{15}N/^1H) = 0.101329118$. NMR spectra were processed with Gifa (version 4.4) (Pons et al., 1996) software utility.

Backbone resonances (^{1}H, ^{15}N and ^{13}C) were assigned using standard three-dimensional (3D) HNCO, HN(CA)CO, HNCA, HN(CO)CA, HNCACB, CBCA(CO)NH (Ikura et al., 1990; reviewed in Sattler et al., 1999), and ^{15}N and/or ^{13}C-edited TOCSY and NOESY experiments (Fesik and Zuiderweg, 1988; Marion et al., 1989; Bax et al., 1990). Aliphatic side-chain assignments were obtained from H(CC)H-TOCSY (Sattler et al., 1999), ^{13}C-edited TOCSY and NOESY experiments, while aromatic side-chain assignments were obtained from 2D homonuclear TOCSY (Rance, 1987) and NOESY (Jeener et al., 1979) experiments. The chemical shifts of the PKBβ-PH domain (major conformation) have been deposited in the BioMagResBank under the accession number BMRB-5778.

Relaxation rate constant measurements were performed on a 0.4 mM protein sample, at 11.7 T (500 MHz). The pulse sequences used to determine ^{15}N $R_N(N_z)$ (R_1), $R_N(N_{xy})$ (R_2), and $^{15}N\{^{1}H\}$NOE values were similar to those described (Peng and Wagner, 1992a,b; Kay et al., 1992; Barthe et al., 1999), experimental parameters and processing were similar to those previously reported in details for other proteins studied in the laboratory (Barthe et al., 1999; Guignard et al., 2000). The ^{15}N longitudinal relaxation rates ($R_N(N_z)$) were obtained from 10 standard inversion-recovery experiments, with relaxation delays ranging from 18 ms to 1206 ms. The ^{15}N transverse relaxation experiments ($R_N(N_{xy})$) were obtained from 10 standard CPMG experiments, with relaxation delays ranging from 16 ms to 144 ms. Both series of experiments were acquired in two single interleaved matrices to ensure uniformity of the experimental conditions. Heteronuclear $^{15}N\{^{1}H\}$ NOE were determined from the ratio of two experiments, with and without saturation. Longer recycling delays (6 s) were used for these experiments in order to obtain a complete relaxation of water magnetization and to reduce effects arising from amide proton exchange.

Molecular modeling calculations

Inter-proton distance restraints obtained from 3D ^{15}N and/or ^{13}C-edited NOESY experiments using mixing times of 100 ms to 150 ms were divided into five classes, according to their intensities. Very strong, strong, medium, weak, and very weak NOEs were then converted into 1.8–2.4, 1.8–2.8, 1.8–3.6, 1.8–4.4 and 1.8–4.8 Å distance constraints. For equivalent protons or non-stereospecifically assigned protons, pseudo-atoms were introduced. Backbone φ and ψ torsion angle constraints were obtained from a database search procedure on the basis of backbone (^{15}N, HN, $^{13}C'$, $^{13}C^{\alpha}$, H^{α}, $^{13}C^{\beta}$) chemical shifts using the program TALOS (Cornilescu et al., 1999), with the ranges of these restraints set to two-times the standard deviation of the predicted value. Amide hydrogen exchange was investigated by recording [^{1}H,^{15}N] HSQC spectra of lyophilized protein freshly dissolved in $^{2}H_2O$. Hydrogen bond restraints were derived using standard criteria on the basis of the amide ^{1}H-^{2}H exchange experiments, $^{13}C^{\alpha}/^{13}C^{\beta}$ secondary shifts and NOE data. When identified, the hydrogen bond was enforced using the following restraints: Ranges of 1.8–2.3 Å for d(N-H,O), and 2.7–3.3 Å for d(N,O).

To determine three-dimensional structures, these distance and dihedral angle restraints were used as input in the standard distance geometry (DG)/simulated annealing (SA) refinement and energy-minimization protocol using the X-PLOR 3.8 program (Brünger, 1993). In the first stage of the calculation, an initial ensemble of 80 structures was generated from a template structure with randomized backbone dihedral angles φ and ψ and extended side chains, using a DG protocol followed by restrained SA and refinement (Nilges et al., 1988). As a result of the thiol titration assay, a covalent disulfide bridge was introduced between the two cysteine residues Cys^{60} and Cys^{77}. Analyzing the obtained structures and comparing them with the NMR data allowed us to identify more NOE restraints, which were introduced into the subsequent calculations. After a number of these processes, 1034 NOE-derived distances (183, intra-residue, 365 sequential, 157 medium-range and 329 long-range), 68 H-bond-derived distances, and 127 dihedral angle restraints (56 φ, 56 ψ, and 15 χ_1) were used as the final input. A calculation was carried out with this input, and the resulting 20 structures with a minimum of restraint violations were submitted to 5000 cycles of restrained Powel energy minimization. The quality of the final ensemble of conformers was assessed using the program PROCHECK (Laskowski et al., 1993). The r.m.s. deviations and visual display were performed with either the program MOLMOL (Koradi et al., 1993), Swiss-Pdb Viewer (Guex and Peitsch, 1997) or INSIGHT 98 (Molecular Simulation Inc., San Diego, CA).

Relaxation data analysis

When the relaxation of the ^{15}N nucleus is predominantly caused by the dipolar interaction with its attached amide proton and by the anisotropy of its chemical shift, the relaxation data can be interpreted in terms of the motion of the ^{15}N-^{1}H vector. Given that the three experimentally determined parameters, $R_N(N_z)$, $R_N(N_{xy})$ and NOE, depend on the spectral density function (Abragam, 1961), the calculation of the spectral density values can be approached by the application of the so-called reduced spectral density mapping, in which the relaxation rates are directly translated into spectral density at three different frequencies (Peng and Wagner, 1992a,b; Farrow et al., 1995; Ishima and Nagayama, 1995a,b; Lefèvre et al., 1996):

$$\begin{bmatrix} J(0) \\ J(\omega_N) \\ < J_{(\omega H)} > \end{bmatrix} = \begin{bmatrix} \frac{-3}{4(3d^2+c^2)} & \frac{3}{2(3d^2+c^2)} & \frac{-9}{10(3d^2+c^2)} \\ \frac{1}{(3d^2+c^2)} & 0 & \frac{-7}{5(3d^2+c^2)} \\ 0 & 0 & \frac{1}{5d^2} \end{bmatrix} \times \begin{bmatrix} R_N(N_z) \\ R_N(N_{x,y}) \\ R_N(H_z \leftrightarrow N_z) \end{bmatrix}, \quad (1)$$

in which

$$d^2 = \left(\frac{\mu_0}{4\pi}\right)^2 \frac{h^2\gamma_N^2\gamma_H^2}{16\pi^2 r_{NH}^6} \quad \text{and}$$

$$c^2 = \frac{1}{3}(\gamma_N B_0)^2(\Delta\sigma)^2,$$

where μ_0 is the permeability of vacuum, h is Planck's constant, γ_H (2.6752×10^8 rad s^{-1} T^{-1}) and γ_N (-2.711×10^7 rad s^{-1} T^{-1}) are the gyromagnetic ratios of the ^{1}H and the ^{15}N nuclei, respectively, and ω_H and ω_N are the ^{1}H and ^{15}N Larmor frequency, respectively; r_{NH} is the internuclear ^{15}N-^{1}H distance (1.02 Å), B_0 is the magnetic field strength, and $\Delta\sigma$ is the difference between the parallel and perpendicular components of the axially symmetric ^{15}N chemical shift tensor, estimated to be -170 ppm (Tjandra et al., 1996; Canet et al., 2001). The cross-relaxation rate $R_N(H_z \rightarrow N_z)$ between ^{15}N and its attached amide proton is correlated with NOE and is calculated using NOE $= 1+(\gamma_H/\gamma_N)\ R_N(H_z \rightarrow N_z)/R_N(N_z)$. The frequency in the average spectral density, $\langle J(\omega_H)\rangle$, may be taken equal to $0.87\omega_H$ (Farrow et al., 1995).

The model-free approach of Lipari and Szabo (1982) was then used to further describe the mobility in terms of specific types of motion. This formalism makes the assumption that overall and internal motions contribute independently to the reorientational time correlation function of ^{15}N-^{1}H vectors and that internal motions occur on a much faster time scale than the global rotation of the molecule. For an isotropically tumbling protein, one obtains:

$$J(\omega) = \frac{2}{5}\left\{S^2\frac{\tau_c}{1+(\omega\tau_c)^2} + (1-S^2)\frac{\tau}{1+(\omega\tau)^2}\right\}, \quad (2)$$

where τ is the harmonics of the overall and the internal (fast) correlation time which pertains to each residue: $\tau^{-1} = \tau_c^{-1} + \tau_f^{-1}$. Fast internal motions are characterized by the square of a generalized order parameter S_f^2, which describes the relative amplitude of internal motions and ranges from 0 to 1, and an internal correlation time τ_f for the internal motions.

For some of the residues, the simple form of Equation 2 turns out to be insufficient to fit the whole set of experimental data. This occurs for residues where observed $J(0)$ values are higher than expected, due to R_{2ex} contributions. In this case, the expression for the observed spectral density at 0 frequency is:

$$J(0) = \frac{2}{5}\left\{S^2\tau_c + (1-S^2)\tau\right\} + \lambda R_{2ex}, \quad (3)$$

where λ is a scale factor : $\lambda = (3/2)[1/(3d^2+c^2)]$. This occurs also when residues exhibit internal motions in a time window close to 1 ns. In this case, the expression for the spectral density function is extended to (Clore et al., 1990):

$$J(\omega) = \frac{2}{5}\left\{S_f^2 S_s^2\frac{\tau_c}{1+(\omega\tau_c)^2} + S_f^2(1-S_s^2)\frac{\tau}{1+(\omega\tau)^2}\right\} \quad (4)$$

with $\tau^{-1} = \tau_c^{-1} + \tau_s^{-1}$, where S_f^2 and S_s^2 are the square of the partial order parameters for fast (picosecond time scale) and slow (τ_s, nanosecond time scale) internal motions, respectively. The square of the generalized order parameter S^2, defined as $S_f^2 S_s^2$, is a measure of the total amplitude of the internal motions. Note that S^2 equals S_f^2 in Equations 2 and 3. Equation 4 assumes that the contribution of the fastest motion to the spectral density function is negligible.

The values of the motional parameters of the individual residues can be derived from the fit of experimental $J(0)$, $J(50$ MHz) and $\langle J(500$ MHz)$\rangle$ using Equations (2), (3) and (4). An iterative non-linear

least-squares algorithm (Press et al., 1986) was employed to further minimize the error function. The 'right' model was selected from χ^2 analysis.

Results and discussion

Structure determination

A major problem confronted in the NMR structure determination of PKBβ-PH was the extremely low stability of this protein in solution. In preliminary experiments recorded at 20 °C on a protein sample dissolved in the conditioning buffer, about 50–60% of the protein precipitated after 3 days, the typical time for recording a 3D [^{1}H,^{15}N]-NOESY-HSQC experiment. Moreover, inspection of [^{1}H,^{15}N]-HSQC spectra showed a strong evolution of the protein during this period of time, essentially revealed by a splitting of most cross-peaks in the fingerprint. We thus performed a micro-drop screening (Lepre and Moore, 1998) in order to optimize the experimental conditions using small amounts of protein. Buffer, PH, salt nature and concentration, and the effect of agonist analogous (inositol-phosphate) were thus rationally examined. This screening procedure demonstrated that the protein was stable for weeks at 4 °C over a very narrow pH range (7.5 ± 0.2 − Tris/HCl 10 mM buffer), at relatively high salt concentration (300 mM NaCl), and in the presence of Ins(1,4,5)P_3 (5 mM). Since peaks were extremely broadened at 4 °C, we choose to work at 13 °C: at this temperature, only 15–25% of the protein precipitated, as judged from the comparison of integrals of 1D ^{1}H spectra recorded on a freshly dissolved sample and after 3 days. Moreover, no spectral evolution was detectable under these conditions. An HSQC spectrum of PKBβ-PH recorded in those conditions is shown in Figure 1.

An extensive set of multidimensional heteronuclear experiments were collected on uniformly ^{15}N- and ^{15}N,^{13}C-labeled protein. Virtually complete backbone resonance assignments and most of the side-chain resonance assignments were completed, except for two peptidic segments: Glu^{59}-Gln^{61} and Arg^{76}-Thr^{87}, and has been reported in detail elsewhere (Auguin et al., 2003). The finger-print obtained from a [^{1}H,^{15}N]-GE-JRSE-HMQC (Szewczak et al., 1993) did not reveal any additional cross-peaks, thus outruling a priori the hypothesis of amide proton solvent exchange – a very efficient mechanism at pH 7.4 – since this experiment is known as particularly suitable for the observation of extremely labile protons. Even though Cys^{60} and Cys^{77} cannot be assigned, these two segments were found linked by a disulfide bridge, as a result of Ellman's assay (see Materials and methods). The loss of these resonances is probably due to an extreme line broadening arising from local conformational exchange on an intermediate timescale induced by the bridge isomerization. Another explanation for the loss of these resonances might be the existence of an hypothetical equilibrium between a monomeric and a dimeric form of the protein in solution through an interaction involving these residues, with a constant rate leading to intermediate exchange of the chemical shifts of the two forms. Note that attempts to displace the conformational (or monomer-dimer) equilibrium toward slow or fast conditions by adjusting the temperature were hampered by intense line broadening or fast protein degradation, respectively. Interestingly, the residues corresponding to the segment Pro^{42}-Pro^{51} exhibited 'minor form' peaks, ranging in intensity from 15–25% of the 'major form' peaks. The minor peaks have been assigned from their proximity to a major peak in the [^{1}H,^{15}N]-HSQC, identification of the amino acid type from the HNCACB, and their placement from the CBCA(CO)NH or ^{15}N-edited HSQC-NOESY. Potential sources for the minor peaks presumably involve proline isomerization states (4 proline residues in this segment), and modification of aromatic ring current effects in the close neighborhood of this peptidic segment.

All experimental restraints used in the final structure calculations are summarized in Table 1. In total, 1229 experimental restraints were employed, representing ≈ 13 restraints per assigned residue. A family of 80 structures was calculated with XPLOR, on the basis of 1034 inter-proton distances, 68 hydrogen bond distances, and 127 dihedral angles. Discarding residues from the two unassigned segments Glu^{59}-Gln^{61} and Arg^{76}-Thr^{87}, and from the segment Pro^{42}-Pro^{51} where different conformations co-exist at equilibrium, the 20 best structures exhibit pair wise r.m.s. deviations of 2.39 ± 0.57 Å and 3.24 ± 0.49 Å with respect to the coordinate positions for the backbone heavy atoms (N, C^{α}, C') and all heavy atoms, respectively (Figure 2). These r.m.s.d. values drop to 0.76 ± 0.19 Å and 1.53 ± 0.16 Å when considering only the secondary structure elements, indicating that these structural elements are well-defined, with maximum violations for upper limits and torsion angles of 0.45 Å and 8.33°, respectively. Excluding unassigned residues and residues belonging to the Pro^{42}-Pro^{51} segment, all residues are observed in the allowed re-

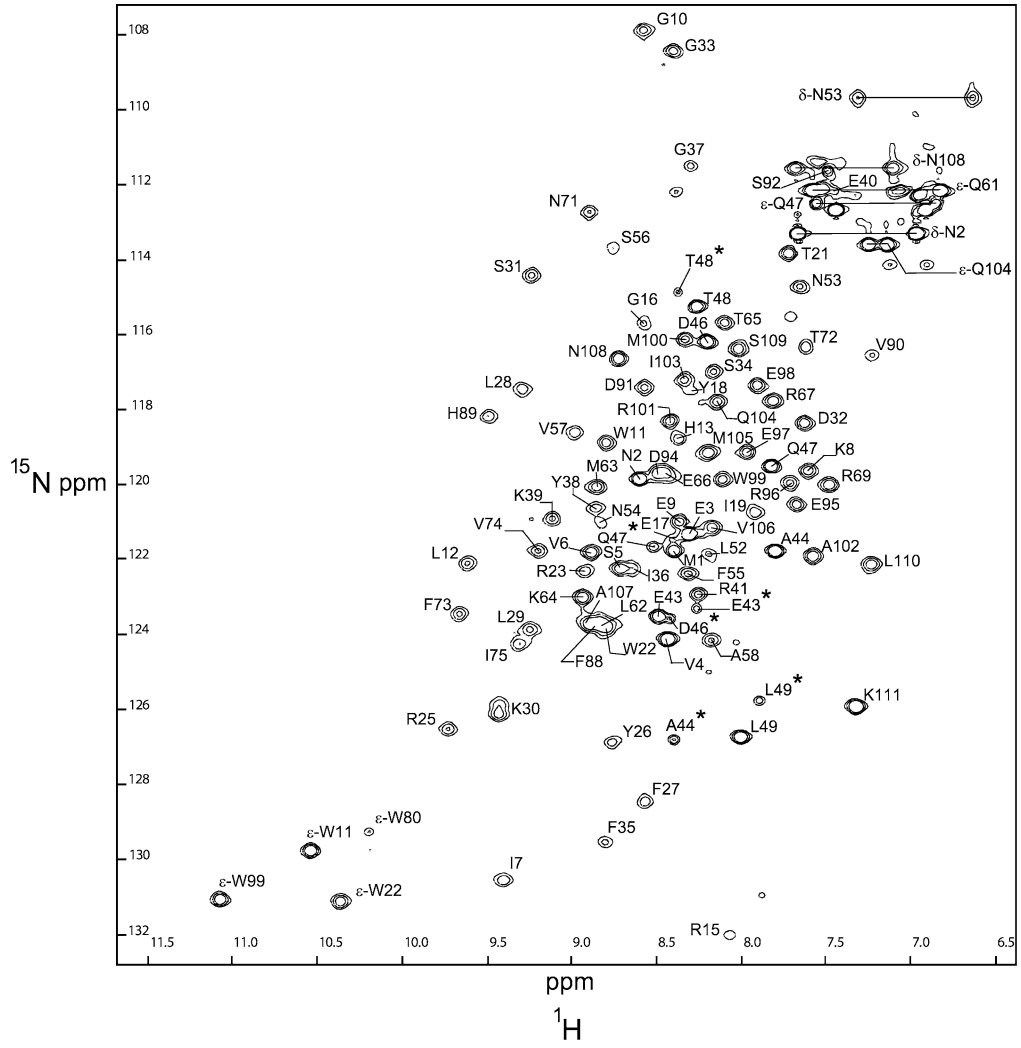

Figure 1. ^{1}H-^{15}N HSQC spectrum of the PKBβ PH domain recorded at 13 °C (400 μM, pH 7.4, 300 mM NaCl and 4 mM In(1,4,5)P_3). The assignment of peaks is indicated with their one-letter amino acid and number. Peaks belonging to the 'minor form' are indicated with stars.

gions of the Ramachandran map. When considering the 20 best models, 84.5%, 13.1%, 1.6% and 0.8% of the assigned residues are in most favored, additional allowed, generously allowed and disallowed regions, respectively, when using PROCHECK (Laskowski et al., 1993). The only residue that appears in disallowed regions is Ala^{44} (14 models), in the Pro^{42}-Pro^{51} peptidic segment, exhibiting strong conformational exchange. Overall, excellent agreement with the experimental data was achieved and good covalent geometry was maintained throughout. This final ensemble of 20 conformers was selected and a model representing the best structure of this ensemble was chosen for purposes of illustration and discussion. The summary of the structural statistics for this 20 conformers is shown in Table 1.

The solution structure of PKBβ-PH is shown in Figure 3: The topology of the fold is typical for PH domains, consisting of seven β-strands forming a β-sandwich flanked at one end by a C-terminal α-helix. More specifically, the first N-terminal four β-strands (β1: Lys^{8}-Arg^{15}; β2: Trp^{22}-Leu^{29}; β3: Phe^{35}-Tyr^{38}; β4: Asn^{53}-Ser^{56}) form the first β-sheet, and the other three β-strands (β5: Gln^{61}-Thr^{65}; β6: Thr^{72}-Arg^{76}; β7: Thr^{87}-Val^{90}) form the second β-sheet. Both sheets have the topology of a β-meander, with the strands occurring in the same order along the sheet as they do in the protein sequence. The two β-sheets pack against each other at an angle of approximately 60°, making

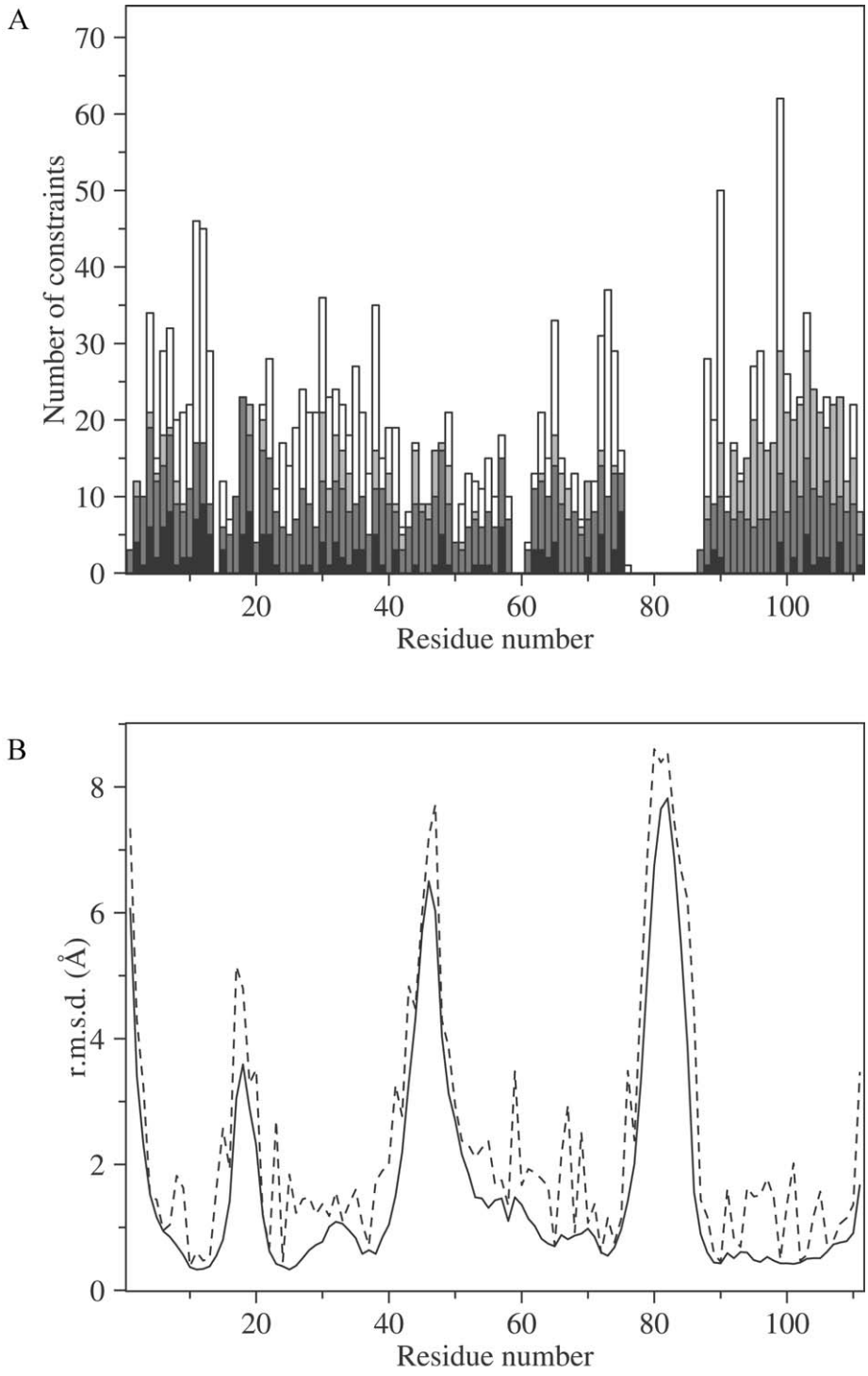

Figure 2. (A) Plot as a function of the amino acid sequence of the number of NOE constraints used in the final structure calculation of the 20 solution structures of PKBβ-PH. NOE categories are shown as follows: Intraresidue, black; sequential, dark shaded; medium range, light shaded; long range, open. NOEs are counted twice. (B) Plots *versus* the amino acid sequence of the mean of the r.m.s. deviations calculated for all backbone heavy atoms (broken line) and for backbone heavy atoms only (plain line) from the 20 NMR structures superimposed over the secondary structure elements.

Table 1. Experimental and structural statistics for the family of 20 structures of PKBβ-PH[a]

No. of distance constraints	
Intraresidue ($i - j = 0$)	183
Sequential ($i - j = 1$)	365
Medium-range ($i - j \leq 4$)	157
Long-range ($i - j > 4$)	329
Total	1034
No. of dihedral angle constraints	
Φ	56
Ψ	56
χ_1	15
Total	127
No. of hydrogen bonds	34
No. of disulfide bridges	1
Mean r.m.s. deviations from experimental restraints	
NOE (Å)	0.028 ± 0.003
Dihedrals (deg)	1.162 ± 0.171
Mean r.m.s. deviations from idealized covalent geometry	
Bonds (Å)	0.003 ± 0.001
Angles (deg)	0.565 ± 0.004
Impropers (deg)	0.360 ± 0.008
Mean energies (kcal.mol^{-1})	
E_{NOE}	12.92 ± 2.33
E_{cdih}	2.68 ± 0.78
E_{vdW}	-340.85 ± 15.42
E_{bond}	21.21 ± 0.79
E_{improper}	19.79 ± 0.89
E_{angle}	165.02 ± 2.41
E_{total}	-602.27 ± 19.94
Pairwise atomic rms differences (Å)	
Residues 1–111 (all) BA[b]/HA[c]	2.39 ± 0.57 / 3.24 ± 0.49
Residues 1–58, 62–75, 88–111 BA[b]/HA[c]	1.82 ± 0.49 / 2.55 ± 0.44
Residues from secondary structures BA[a]/HA[b]	0.76 ± 0.19 / 1.53 ± 0.16

[a]For these calculations, the XPLOR all-hydrogen force fields topoallhdg and parallhdg were used. The final minimization of the 20 structures was carried out with force constants of 15 kcal mol^{-1} Å^{-2} and 50 kcal mol^{-1} rad^{-2} for the NOE and dihedral angle potentials, respectively.
[b]Backbone atoms.
[c] All heavy atoms.

contact at only two (close) corners. One of these close corners is spanned by strand β1, which contributes to both sheets of the β-sheet. The other close corner is completed by the turn between β4 and β5. The C-terminal amphipatic α-helix (Pro^{93}-Ser^{109}) is packed into a gorge below the plane of the strands β1 and β2 in parallel to strand β5, capping one top of the sandwich. All these elements of secondary structure are adequately defined by long- and medium-range NOEs and H-bond networks, as well as by the carbon and proton secondary chemical shifts. The stability of this scaffold is ensured by a hydrophobic core consisting of Leu^{12} on β1, Phe^{27}, Leu^{29} on β2, Phe^{35} on β3, Phe^{55}, Val^{57} on β4, Leu^{62} on β5, Phe^{73}, Ile^{75} on β6, Phe^{88}, Val^{90} on β7, and Trp^{99}, Ile^{103} and Val^{106} on the α-helix. The other face of the sandwich presents three loops (β1/β2, β3/β4 and β6/β7) of variable length. Since these three loops were found to be the most variable regions (in length or in sequence) in early alignments of PH domains (Haslam et al., 1993; Mayer et al., 1993; Musacchio et al., 1993; Gibson et al., 1994), they were termed the 'variable loops' VL1, VL2 and VL3, respectively, by analogy with immunoglobulin-like domains. These loops ap-

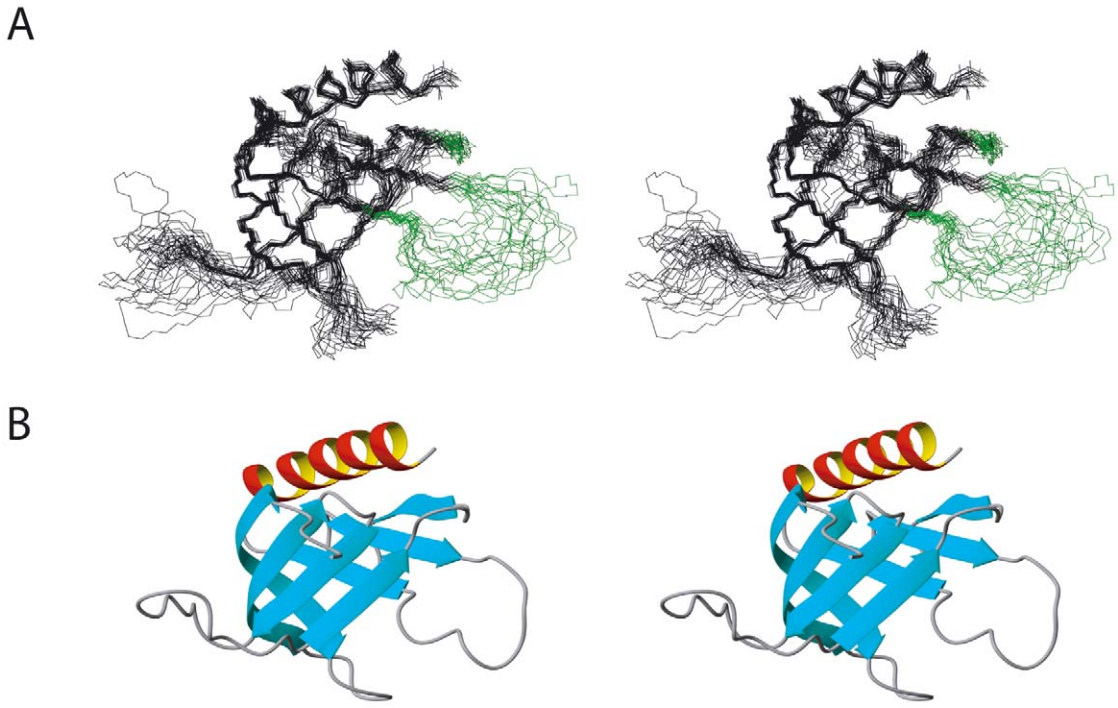

Figure 3. (A) Stereoview of the final 20 NMR structures of PKBβ-PH superimposed on the backbone atoms of regular secondary structure elements. Only backbone atoms (Cα, C′ and N) are displayed. The unassigned – and hence unrestrained - peptide segments (Glu^{59}-Gln^{61} and Arg^{76}-Thr^{87}) are colored in green. (B) Ribbon stereodiagram of the lowest energy structure of PKBβ-PH showing the secondary structure elements. The coordinates of the solution structure of PKBβ-PH have been deposited to the Protein Data Bank (code: 1p6s (20 calculated structures)).

pear as the most ill defined structural elements in the solution structure of PKBβ-PH, especially for VL3 (β6/β7), for which no assignment was possible, and VL2 (β3/β4). The technical difficulties in observing the residues belonging to VL3 probably arise from conformational fluctuation in this region, leading to line broadening from exchange on an intermediate time scale. As previously noted, this is further supported by the presence of a disulfide bridge linking β5 to β6, whose isomerization can promote such motions. In VL2 (β3/β4), most residues exhibit split resonances, suggesting the existence of a minor conformation (15–25%, as judged from the peak intensities) in slow exchange with the major one. This can be attributed to the striking richness in proline residues of this segment, and inferred to proline cis/trans isomerization. Note that for some residues, the two conformations can display very different chemical shifts. Indeed, the $^{15}N/^{1}HN$ chemical shifts measured for residues Ala^{44}, Asp^{46} and Gln^{47} in the major conformation are 121.8 ppm/7.78 ppm, 116.1 ppm/8.16 ppm, and 119.5 ppm/7.79 ppm, respectively, whereas those measured in the minor conformation are 126.9 ppm/8.38 ppm, 123.6 ppm/8.39 ppm, and 121.6 ppm/8.48 ppm. Such important effects can be partly explained by the vicinity of the aromatic side-chain of Tyr^{38} on the β-sandwich, facing VL2 that can promote ring currents of different intensity, depending on the conformation of VL2. Interestingly, these loops are ill defined in most of the solution structures of PH domains, suggesting an intrinsic flexibility that could be of functional importance. For instance, the residues of VL3 cannot be assigned in the NMR study of the PH domain of dynamin (Fushman et al., 1995), even though conformational fluctuations in this particular case cannot be attributed to disulfide bridge isomerization.

Backbone dynamics analysis

Figure 4 shows the two relaxation rate constants and the heteronuclear NOEs at stationary state that were measured for 72 of the 104 non-proline residues of PKBβ-PH, as well as the three corresponding reduced spectral densities $J(0)$, $J(\omega_N)$ and $\langle J(\omega_H)\rangle$ obtained from Equation 1. The low $J(0)$ values for the terminal

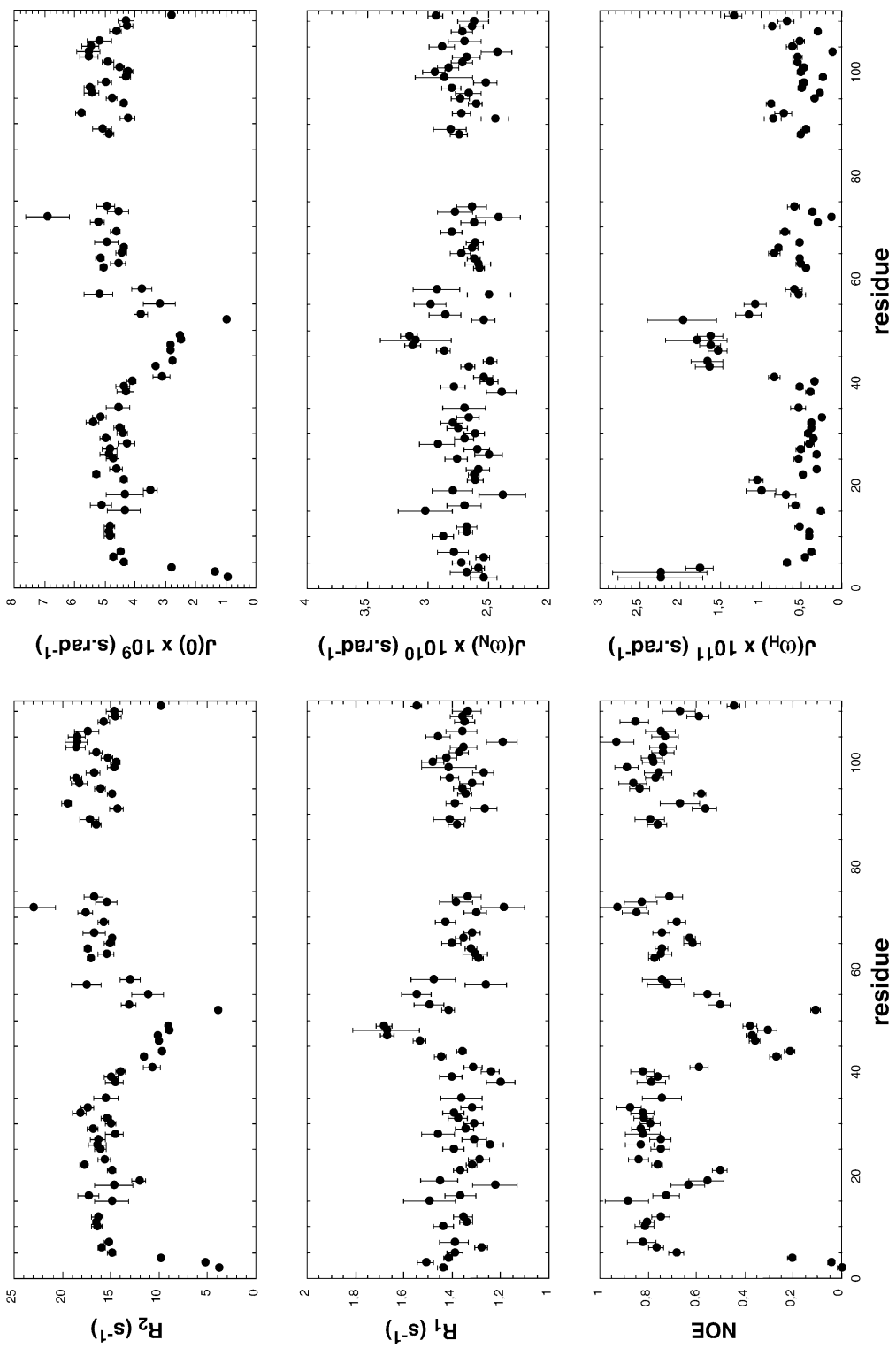

Figure 4. Relaxation rates and $^{15}N\{^{1}H\}$NOEs (left) as a function of the sequence obtained for PKBβ-PH (400 μM, pH 7.4, 13 °C, 300 mM NaCl, and 4 mM In(1,4,5)P_3), and corresponding values of the three spectral densities (right) calculated from Equation 1.

residues and, to a lesser extent, those for the peptidic segments Gly^{16}-Thr^{21} and Arg^{41}-Leu^{52}, are indicative of an increased flexibility. These two segments correspond to the variable loops VL1 and VL2. In these regions, reduced values of $J(0)$ are compensated for by high values of $\langle J(\omega_H)\rangle$, supporting the fact that the higher values of r.m.s.d. observed in these ill-defined regions are due to intrinsic flexibility rather than to a lack of structural data. Low $\langle J(\omega_H)\rangle$ values for the rest of the protein indicate restricted flexibility on fast time-scales. At 50 MHz, $J(\omega)$ values exhibit a pattern opposite to that observed for $J(0)$: a slight increase is observed for NH vectors located on VL2 and, to a lesser extent, on VL1. This indicates that $J(\omega_N)$ is slightly greater than the isobestic frequency, where the contribution of $J(\omega)$ is independent of the internal mobility. Thr^{72} and, to a lesser extent, Val^{57} exhibit significantly higher values of $J(0)$, while $J(\omega_N)$ and $\langle J(\omega_H)\rangle$ for these residues are not smaller than the mean values. This is in favor of the existence of slow movements in the micro- to millisecond range around these residues. These processes increase the value of the spectral density function in a very narrow frequency range, from zero to a few kilohertz, but have no influence at higher frequencies in the megahertz range. It is noteworthy that these fluctuations in the slow frequency regime occur either around aromatic residues (Phe^{73} and Phe^{55}) or cysteine residues (Cys^{60}-Cys^{77}). It is known that small displacements of the aromatic rings could give rise to large chemical shift variations (via ring-current effects), leading to an efficient adiabatic relaxation pathway. Around cysteine residues, a similar contribution to relaxation can arise from slow isomerization of the cysteine side chains engaged in disulfide bonds (Szyperski, 1993). This relaxation pathway contributes to transverse relaxation (R_{2ex} term) and leads to an increase of the spectral density $J(0)$. Similar mechanisms might be invoked to explain the dispersion observed for the $J(0)$ value in the C-terminal helical segment. Of course, no information can be obtained for the unassigned variable loop VL3, even though we suspect, from previously discussed considerations, a very complex dynamical behavior in this peptidic segment, involving fluctuations on an intermediate time scale.

The mapping of spectral densities $J(\omega)$ for each backbone NH bond provides the intrinsic dynamic information from the relaxation data – without any assumption for the motional model – upon which a variety of motional models may be evaluated. Since both values of $J(\omega_N)$ and $J(\omega_H)$ decrease for almost all NH vectors with increasing ω_N and ω_H frequencies, respectively, the description of the spectral densities as sums of Lorentzians appears qualitatively reasonable for PKBβ-PH. Adequate fits of $J(\omega)$ are therefore expected using the model-free formalism proposed by Lipari and Szabo (1982). On the other hand, the ratio of the principal components of the average inertia tensor for the backbone atoms on the average structure of PKBβ-PH was determined to be (1/0.82/0.71). These numbers suggest that the overall rotation of the protein is expected to have only a small degree of anisotropy that may not have a strong influence at least on the order parameters values (Tjandra, 1995). Thus, we do not make any attempt to introduce this contribution in the motional model.

The global value of the overall rotational correlation time τ_c was taken as the average of the values obtained independently for all residues which were well parameterized (low χ^2) by the 'simple' Lipari–Szabo formalism (Equation 2) and showed order parameters higher than 0.70. This procedure leads to a correlation time equal to 12.9 ns, fully compatible with the size of a monomeric form of the protein in solution at this relatively low temperature. As a first result, we can discard the hypothesis of a monomer-dimer equilibrium through an interaction involving residues belonging to VL3. Once the overall tumbling time τ_c has been determined, local model-free parameters were obtained by using either the 'simple' (with or without R_{2ex} contributions) or the 'extended' Lipari–Szabo formalisms (see Materials and methods). The micro-dynamical parameters S^2, S_s^2, S_f^2, τ_s, τ_f, and R_{2ex} obtained from this analysis are plotted in Figure 5. The 'simple' Lipari–Szabo model suffices to describe the motion of most NH vectors. The 'extended' model was necessary to correctly describe the dynamics of the N- and C-terminal residues, for NH vectors located in VL2 and for the residue Ile^{19} in VL1. The use of the 'extended' model was fully justified by the statistics, and, supporting the choice, reasonable values of τ_s (1.3 $\pm$ 0.3 ns) were observed when it brought undeniable improvements of the fit. Interestingly, while S_s^2 and S_f^2 decrease concomitantly for residues located in the disordered N- and C-terminus, the decrease observed for the generalized order parameter ($S_s^2 \times S_f^2$) in VL2 arises uniquely from the drop of S_s^2 values. This is in favor of a hinge motion for this loop on the subnanosecond time scale, since the high values observed for S_f^2 indicate significant restriction of the fast motions of the NH vectors, consistent with a reasonably well-organized structure for this loop. Superimposed

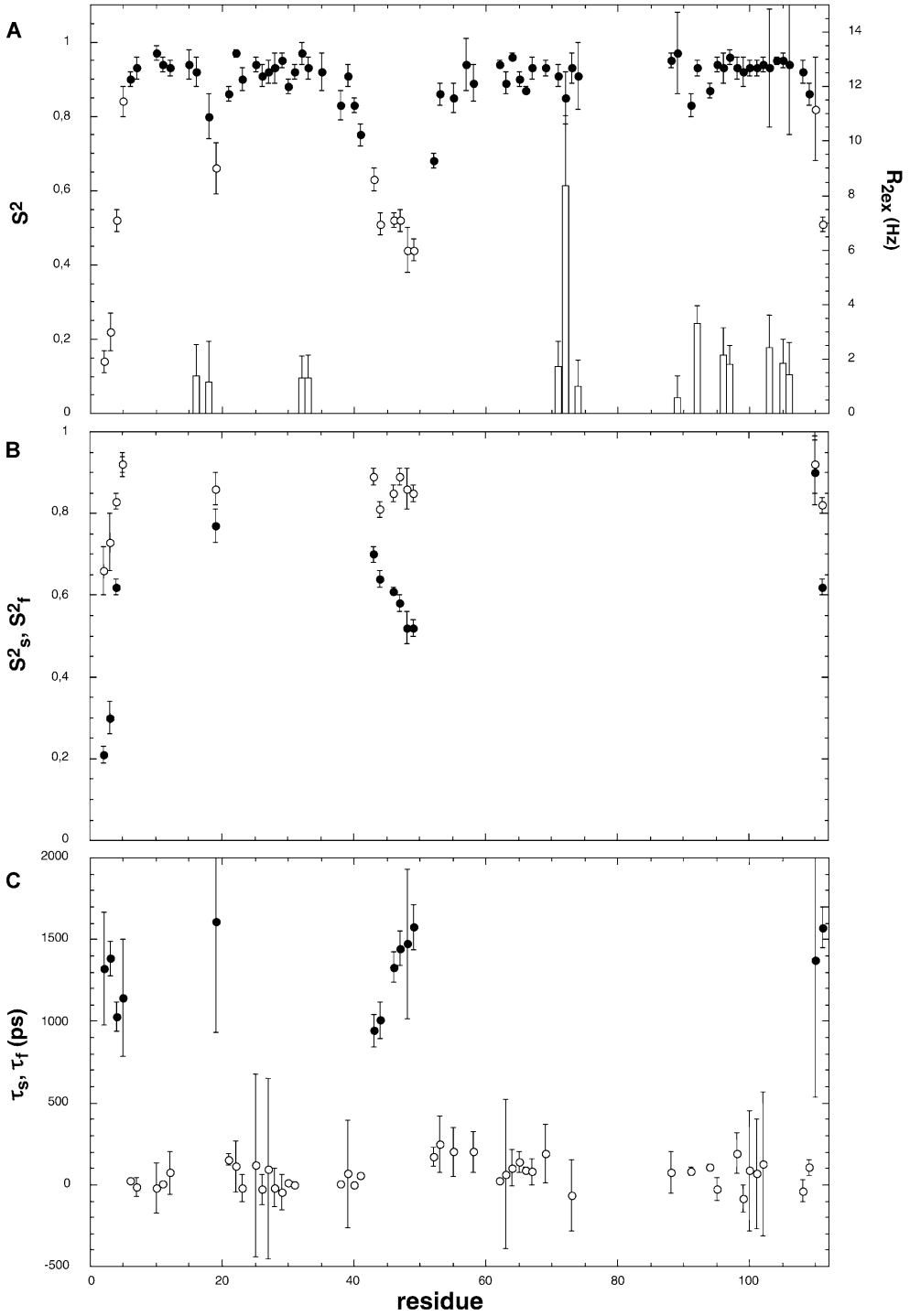

Figure 5. Model-free micro-dynamical parameters (S^2, S^2_s, S^2_f, τ_s, τ_f) and exchange contribution (R_{2ex}) to the transverse relaxation rate for the NH vectors of PKBβ-PH. (A) Generalized order parameter S^2 and R_{2ex}. The two parameter spectral density function (Equation 2) has been used excepted when S^2 are plotted as open circles: for these residues, the extended Lipari–Szabo formalism has been used (Equation 4) and the value of the order parameter is given as $S^2_f \times S^2_s$ R_{2ex} contribution is plotted as open bars for residues where the use of Equation 3 was necessary to correctly parameterized $J(0)$ in Equation 2. (B) Partial order parameters S^2_s (plain circles) and S^2_f (open circles) obtained for residues fitted with the extended Lipari–Szabo formalism. (C) τ_f (plain circles) and τ_s were obtained from Equation 2 (simple model) or Equation 3 (extended model), respectively.

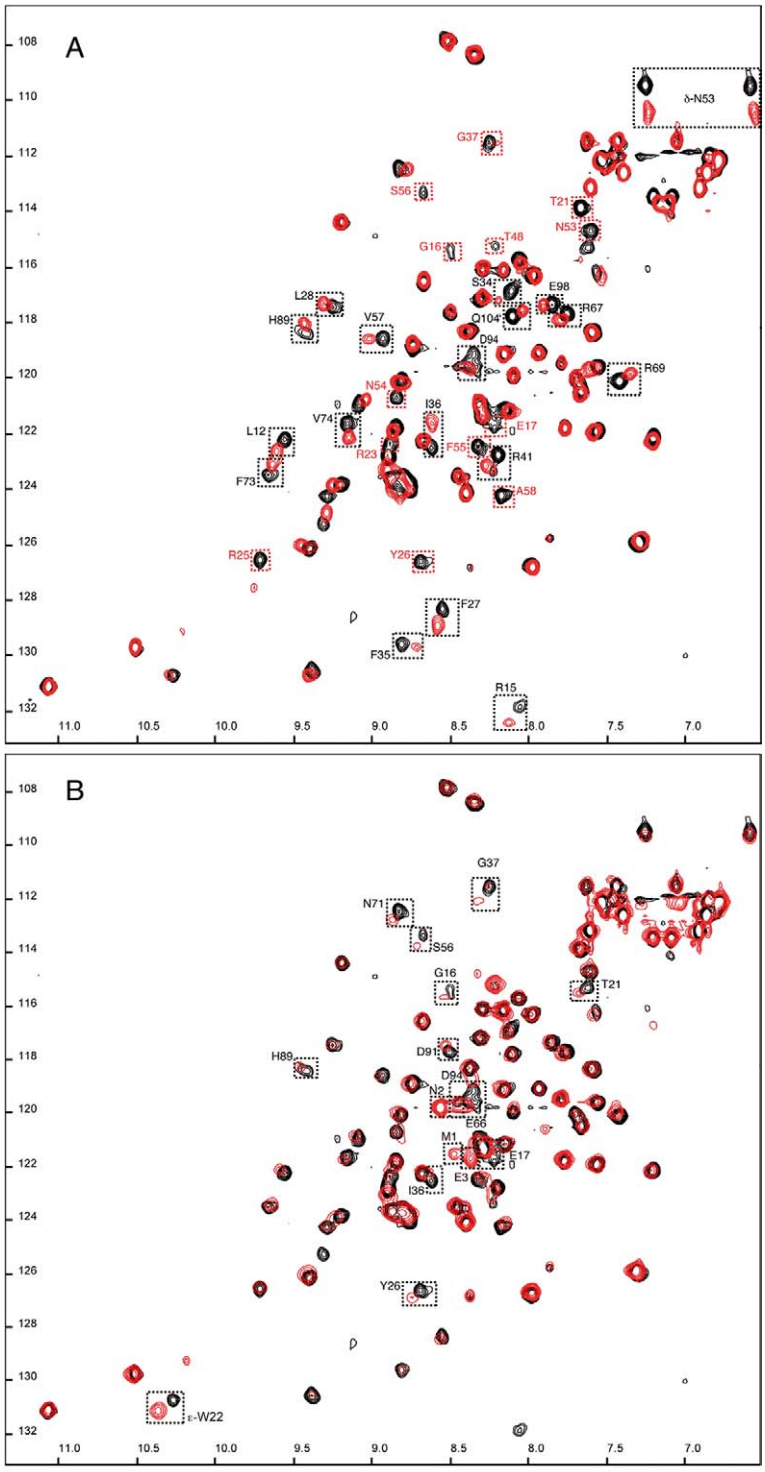

Figure 6. Superimposition of HSQC spectra recorded in an inositol-phosphate 'free' sample of PKBβ-PH (400 μM, pH 7.4, 4 °C, 300 mM NaCl) in solution (black contours) and in similar conditions but in presence of (A) 4 mM Ins(1,3,4,5)P_4 (IP_4) and (B) 4 mM Ins(1,4,5)P_3 (IP_3) (red contours). Cross-peaks exhibiting line broadening upon addition of IP_4 are indicated with red squares and are labeled in red. Cross-peaks exhibiting shifts upon addition of IP_3 or IP_4 are indicated with black squares and are labeled in black.

on this hinge motion, proline isomerization gives rise to an equilibrium between a major and minor conformations, as revealed by the existence of minor peaks for residues belonging to VL2 in the HSQC spectrum. This conformational equilibrium involves slow motions on the chemical shift scale. On the other hand, several residues (Gly^{16}, Tyr^{18} in VL1, Asp^{32}, Gly^{33} in the β2/β3 loop, Asn^{71}, Thr^{72} and Val^{74} in β6, His^{89}, Ser^{92} in the loop joining β7 to the α-helix, and Arg^{96}, Glu^{97}, Ile^{103}, Met^{105}, Val^{106} in the α-helix) exhibit significant positive values of R_{2ex}, suggesting the presence of motions on the microsecond to millisecond time scale. All these residues are in close proximity of an aromatic residue, either through the sequence or through space, so that the R_{2ex} contributions can be explained readily by ring current fluctuations associated with slow motions. Note that correct quantification of exchange phenomena implies performing other experiments, such as recording relaxation data at different field strengths (Guignard et al., 2000; Canet et al., 2001) or measuring the rotating frame relaxation times as a function of the spin-lock power (Szyperski et al., 1993; Blackledge et al., 1993). In the variable loop VL1, the residue Ile^{19} undergoing slow internal motion on the sub-nanosecond time scale remains close to residues where significant positive values of R_{2ex} are measured. This suggests that different internal motions on the sub-nanosecond to the micro- or even millisecond time scale may contribute to the dynamics of the NH vectors in this loop. It should be mentioned at this point that the estimated extended model-free parameters depend on the assumption that the exchange contribution to the transverse relaxation rate is negligible. If it is not true, the contribution of slow motions to the relaxation may be underestimated. A similar behavior should be suspected for the variable loop VL3: Slow exchange motions are detectable at the two extremities, suggesting that the unassigned NH vectors in this loop are probably engaged in complex motions, on an intermediate time scale.

Binding to inositol phosphates

It has been previously reported that the PH domain of PKB binds with high affinity and specificity the lipid second messengers PtdIns(3,4)P_2 and PtdIns(3,4,5)P_3, the products of agonist-stimulated PI3K (James et al., 1996; French et al., 1997). In our first attempts to stabilize the protein in solution, we tested the effect of Ins(1,3,4,5)P_4 (IP_4: The head group of PtdIns(3,4,5)P_3), used for the resolution of the crystal structure of PKBα-PH (Thomas et al. 2002), and Ins(1,4,5)P_3 (IP_3), an analogous of the phosphatidylinositide head-group that presents a significant, even low, affinity for related PH domains (Ferguson et al., 2000). Both compounds were found to stabilize the protein in the microdrop assays, and their effects on the NMR spectra were investigated further.

The binding of IP_4 to PKBβ-PH

Addition of IP_4 to PKBβ-PH resulted essentially in the progressive loss of several resonances, indicative of an intermediate exchange behavior, or in the progressive shift of other resonances, indicative of a fast exchange behavior, in the resulting HSQC spectra. Mapping of those residues with perturbed resonances onto the solution structure of PKBβ-PH is displayed for the entire molecule in Figure 6A, where a superimposition of free and IP_4-bound PKBβ-PH at saturation (0.4 mM protein/4 mM IP_4) HSQC spectra is shown. With the exception of Gly^{37} (β3) and Thr^{48} (VL2), line broadening concerns the resonances of amide groups located in the variable loop VL1 (Gly^{16}, Glu^{17}, Thr^{21}), the β2-strand (Arg^{23}, Arg^{25}, Tyr^{26}), and the β4-strand (Asn^{53}, Asn^{54}, Phe^{55}, Ser^{56}, Ala^{58}) (Figure 7A). These spectral modifications are consistent with the IP_4 binding site found in the crystal structure, since they concern residues either directly involved in the interaction with phosphate groups in the crystal structure of the complex, or in close proximity. Indeed, in the crystal structure of IP_4-bound PKBα-PH, this binding site is located in a pocket formed by VL1 and VL2 where the phosphate groups of IP_4 interact with either amide backbone protons or the side-chain of basic residues: the D1 phosphate interact with Arg^{23} and the backbone nitrogen of Ile^{19}, the D3 phosphate interacts with the side chains of Lys^{14}, Arg^{23}, Arg^{25} and Asn^{53}, the D4 phosphate interacts with Lys^{14}, Asn^{53} and Arg^{86}, and the D5 phosphate does not interact with any protein atoms in the binding pocket and is solvent exposed. In addition, the amide resonances of several amide groups belonging to residues located in or close to the binding site exhibited significant shifts: Leu^{12} and Arg^{15} in VL1, Phe^{27} and Leu^{28} in β2, and Val^{57} in β4. Remarkably, a very important shift was also observed for the δ-NH_2 side chain resonances of Asn53, confirming the direct involvement of this basic side chain (that bound both the D3 and D5 phosphates in the crystal structure) in the binding site. Interestingly, the complex dynamical behavior experienced by VL2 seems not drastically affected by IP_4 bind-

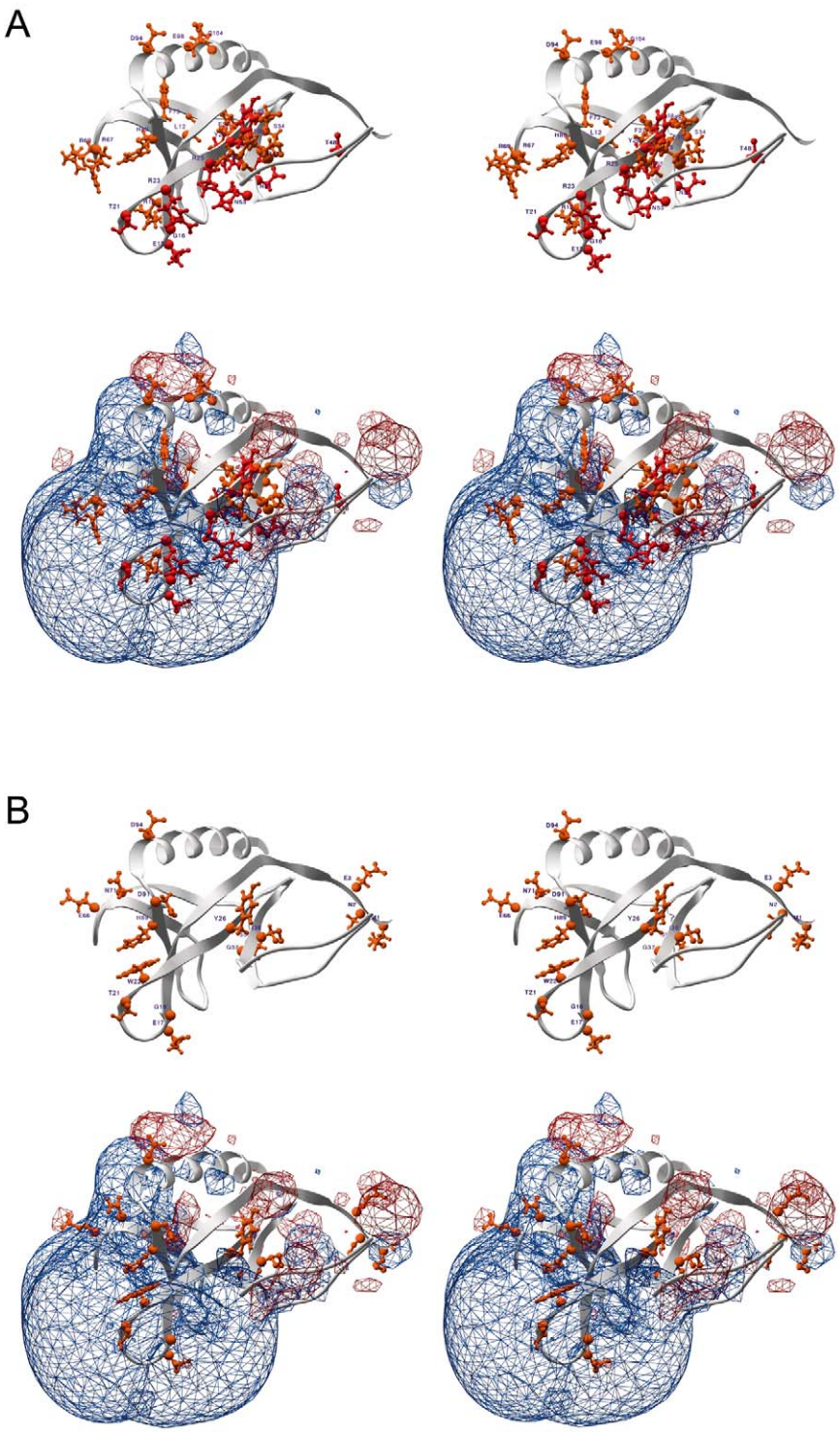

Figure 7. Ribbon stereodiagrams of the structure of PKBβ-PH. The side chains of residues exhibiting perturbed resonances upon addition of IP_4 (A) or IP_3 (B) are reported and colored in red (line broadening) or orange (shifts). In each panel, a colored (−2.5 kT (red) and +2.5 kT (blue)) electrostatic potential map has been calculated and added to the corresponding stereodiagram (bottom view) using the program Swiss-Pdb Viewer (Guex and Peitsch, 1997).

ing, since we observed the same minor peaks in the 'free' and in the 'bound' HSQC spectra, suggesting that the conformational equilibrium is – at least qualitatively – not disrupted when adding of IP_4. On the other hand, other significant shifts were observed for resonances of residues remote from the binding site: Phe^{27} and Leu^{28} in β2, Ser^{34}, Phe^{35}, and Ile^{36} in β3, Arg^{41} in VL2, Arg^{67} and Arg^{69} in the β5/β6 loop, Phe^{73} and Val^{74} in β6, His^{89} in β7 and Asp^{94}, Glu^{98} and Gln^{104} in the C-terminal α-helix. These perturbations might be explained by long range effects due to slight rearrangements of the pocket upon binding, probably propagated via ring-current effects, given the particularly richness in aromatic residues of the molecule core. Another explanation could be non-specific interactions between the phosphate groups on the inositol ring and the solvent exposed side chains of basic residues: this could explain the shifts experienced by residues located in the highly basic pocket delimited by VL1 and VL3 (Figure 7A). PKBβ-PH binds IP_4 with nanomolar affinity: with such a strong affinity, slow exchange conditions are expected for residues bound to IP_4. The intermediate exchange behavior observed in solution might be attributed to subtle rearrangements of the multiple interactions competing for the linking of the sugar in the binding site in the protein. Such a dynamical process can promote spectral line broadening, and remains compatible with the high affinity of the ligand. As a result of the line broadening experienced by many resonances in the HSQC spectra, investigation of the structure of PKBβ-PH in complex with IP_4 was not investigated further.

The binding of IP_3 to PKBβ-PH

As depicted in Figure 6B, where a superimposition of free and IP_3-bound PKBβ-PH at saturation (0.4 mM protein/4 mM IP_3) HSQC spectra is reported, the binding of IP3 to the protein resulted mainly in resonance shifts, indicative of fast exchange conditions and consistent with the low affinity constant measured for the interaction of IP_3 with closely related PH domains. As observed when adding IP_4, some amide cross-peaks of residues that have been found involved in the binding site in the crystal structure (namely Gly^{16}, Glu^{17} and Thr^{21} in VL1, Tyr^{26} in β2, Ser^{56} in β4) exhibited significant shifts upon addition of IP_3. Nevertheless, the δ-NH2 resonances of Asn^{53} appeared unchanged, even after addition of a 40-fold excess of IP_3 (data not shown). This residue tightly binds the D3 (absent in IP_3) and D4 phosphate groups of IP_4. In contrast, the indole NH resonances of Trp^{22} displayed a very important shift upon addition of IP_3. This side chain resides on the β2-strand and points to the VL3 loop, on the opposite side of the IP_4 binding pocket. VL1 and VL3 form another highly basic pocket that might bind (with low affinity) the IP_3 molecule. This is supported by the shifted resonances of several residues in this area (Asn^{71}, His^{89}, Asp^{91}, Asp^{94}) (Figure 7B), whereas residues belonging to the β4-strand appear virtually unaffected by the binding of IP_3, contrary to what is observed upon addition of IP_4. Note that because the residues of VL3 were not assigned, the description of this putative site by chemical shift mapping could be incomplete. At high IP_3 concentration (40-fold excess), others residues appeared affected in this pocket (Arg^{15}, Tyr^{18}, Ile^{19}, Arg^{69}, Thr^{72}, Val^{74}), but also in more distant areas: Trp^{11}, Leu^{12} in β1, Arg^{25}, Tyr^{26} in β2, Ile^{36}, Gly^{37} in β3, Thr^{48} in VL2, Asn^{54}, Phe^{55} in β4, Glu^{66}, Arg^{67} in the β5/β6 loop, Arg^{96}, Glu^{98}, Trp^{99}, Ala^{102} in the C-terminal helix (data not shown). Due to the low affinity of the PH domain for IP_3, long-range effects consecutive to backbone rearrangements upon binding are highly improbable, and should concern a relatively restricted area around the binding site. Supporting this assumption, the dynamics of VL1 and VL3 were not perturbed upon addition of IP_3. Thus, no additional peaks are observed in the HSQC spectrum of the 'complex', indicating that VL3 retains intermediate exchange conditions in the presence of IP_3. In the case of VL1, it is difficult to conclude if the addition of IP_3 modifies or not the dynamics, since the dynamics study of the 'free' protein in solution cannot be undertaken, due to its very low stability. Nevertheless, the low S^2 values observed in the 'complex' are indicative of a high flexibility for this loop in the presence of IP_3, suggesting that the VL1 dynamics is not drastically affected upon IP_3 binding. Even though slight backbone rearrangements cannot be completely discarded, we believe rather that, concomitantly to the binding to a low-affinity binding site, IP_3 might bind in a non-specific manner to a more extended surface on the molecule. Supporting this assumption, most of the residues experiencing shifted resonances reside on the basic face of the PH domain. In addition, the resonances of the N-terminal residues were narrowed and shifted upon addition of IP_3, suggesting stabilization by an electrostatic interaction between phosphate groups and the NH_2 terminal group. This non-specific association could also provide an explanation for the observed stabilization of PKBβ-PH in solution in the presence of IP_3. PKBβ-PH, as PKBα-PH, is a highly

polar molecule (see Figure 7, bottom), and this high polarity favors protein aggregation in solution. IP_3 could prevent protein aggregation by screening the positive charges in the basic face of the protein.

Concluding remarks

The structure of the PH domain of PKBβ presents the canonic fold observed for other PH domains, either in solution or in the crystal. Since atomic coordinates are not still available from the PDB, accurate comparison of the crystal structure of PKBα-PH and the present solution of PKBβ-PH cannot be undertaken, but some conclusions can be drawn readily from the data reported in the paper of Thomas et al. (2002). As expected, the overall fold of the two proteins is essentially the same. In addition, the polarity of the molecule is preserved, with VL1 and VL2 on one face of the sandwich forming a bowl lined with basic residues, whereas the other face of the sandwich, capped with the α-helix, displays essentially negative charges. Major differences concern VL2 and VL3. The loop VL3 appears well defined in the crystal structure, whereas most of its residues are unassigned in the NMR study. The sequence of VL3 is strictly identical in the two protein isoforms, with the exception of Val^{74} replaced by the homologous isoleucine residue in PKBα-PH. This suggests that the structural differences observed for this loop between the solution and the crystal structure arise essentially from differences in dynamics. Since we do not have access either to the B-factors or to the packing of the protein in the crystal mesh, it is impossible to conclude whether VL3 displays a substantial flexibility in the crystal, or if the crystal packing stabilizes its structure. On the other hand, both the sequence and the structure of VL2 appear markedly different between the two proteins. In PKBα-PH, VL2 contains a high concentration of negatively charged residues (Glu40, Asp44, Asp46, and Glu49) that occupy one side of a short helix and face away from the PH domain core, toward the solvent. In PKBβ-PH, VL2 displays only three negatively charged residues (Glu40, Glu43, and Asp46), two of them being strictly conserved between the two isoforms. The main difference is the striking richness in proline residues of VL2 in PKBβ-PH: Four prolines are present in this 10-residues peptide segment (Pro^{42}, Pro^{45}, Pro^{50} and Pro^{51}), whereas only two are conserved in PKBα-PH (Pro^{42} and Pro^{51}). Even if the structure of VL2 is ill defined in solution, this extreme richness in proline residues appears hardly compatible with a helical structure. As revealed by the ^{15}N relaxation study, the variable loops VL1 and VL2 appear very mobile in solution, so that their poor structural definition (especially in case of VL2) cannot be inferred to a lack of structural constraints but rather to their intrinsic flexibility. VL2 experiences very complex motions in solution: Superimposed on a sub-nanosecond hinge motion, the splitting of the ^1H and ^{15}N chemical shifts of most amide groups in this loop is indicative of a conformational equilibrium, probably due to proline isomerization. As a result of the chemical shift mapping study, titration of PKBβ-PH with IP_4 gave results compatible with those gained from the crystal structure: all residues exhibiting perturbed resonances are found in or near the high-affinity IP_4 binding site in the crystal structure of the complex. Interestingly, a similar approach suggested a putative different low-affinity binding site for IP_3. In addition, IP_3 might bind in a non-specific manner the basic residues located in the positively charged face of the protein. This screening effect could explain the stabilization of PKBβ-PH in solution by IP_3.

Acknowledgements

We are grateful to the 'Association pour la Recherche sur le Cancer' for a research grant. D. Auguin is supported by the 'Fondation pour la Recherche Medicale', M. Noguchi by 'Cancer Reseach Investigator Award'. The authors are specially grateful to F. Hoh and M.P. Strub for their assistance in protein expression and labeling, and to C. Royer for the critical reading of this paper.

References

Abragam A. (1961) *Principles of Nuclear Magnetism*, Oxford Science Publication, Clarendon Press, Oxford.

Alessi, D.R., Andjelkovic, M., Caudwell, B., Cron, P., Morrice, N., Cohen, P. and Hemmings (1996) *EMBO J.*, **15**, 6541–6551.

Andjelkovic, M., Jones, P.F., Grossniklaus, U., Cron, P., Scier, A.F., Dick, M., Bibe, G. and Hemmings, B.A. (1995) *J. Biol. Chem.* **270**, 4066–4075.

Auguin, D., Barthe, P., Augé-Sénégas, M.-T., Hoh, F., Noguchi, M. and Roumestand, C. (2003) *J. Biomol. NMR*, **27**, 287–288.

Barthe, P., Chiche, L., Declerck, N., Delsuc, M.A., Lefèvre, J.F., Malliavin, T., Mispelter, J., Stern, M.-H., Lhoste, J.M. and Roumestand, C. (1999) *J. Biomol. NMR*, **15**, 271–288.

Bax, A., Ikura, M., Kay, L.E., Torchia, D.A. and Tschudin, R. (1990) *J. Magn. Reson.*, **86**, 304–318.

Bellacosa, A., Testa, J.R., Staal, S.P. and Tsichlis, P.N. (1991) *Science*, **254**, 274–277.

Blackledge, M.J., Brüschweiler, R., Griesinger, C., Schmidt, J.M., Xu, P. and Ernst, R.R. (1993) *Biochemistry*, **32**, 10960–10974.

Brünger, A.T. (1993) *X-PLOR (Version 3.1): A system for X-Ray Crystallography and NMR*, 3.1 edit, Yale University Press, New Haven, CT.

Canet, D., Barthe, P., Mutzenhardt, P. and Roumestand, C. (2001) *J. Am. Chem. Soc.*, **123**, 4567–4576.

Cantrell, D. (2002) *Immunology*, **14**, 19–26.

Clore, G.M., Driscoll, P.C., Wingfield, P.T. and Gronenborn, A.M. (1990) *Biochemistry*, **29**, 7387–7401.

Coffer, P.J. and Woodgett, J.R. (1991) *Eur. J. Biochem.*, **201**, 475–481.

Cornilescu, G., Delaglio, F. and Bax, A. (1999) *J. Biomol. NMR*, **13**, 289–302.

Datta, S.R., Brunet, A. and Greenberg, M.E. (1999) *Genes Develop.*, **13**, 2905–2927.

Farrow, N.A., Zhang, O., Szabo, A., Torchia, D.A. and Kay, L.E. (1995) *J. Biomol. NMR*, **6**, 153–162.

Ferguson, K.M., Kavran, J.M., Sankaran, V.G., Fournier, E., Isakoff, S.J., Skolnik, E.Y. and Lemmon, M. (2000) *Mol. Cell*, **6**, 373–384.

Fesik, S.W. and Zuiderweg, E.R.P. (1988) *J. Magn. Reson.*, **78**, 588–593.

Frech, M., Andjelkovic, M, Ingley, E., Reddy, K.K., Falck, J.R. and Hemmings, B.A. (1997) *J. Biol. Chem.*, **272**, 8474–8481.

French, S.W., Shen, R.R., Koh, P.J., Malone, C.S., Mallick, P. and Teitell, M.A. (2002) *Biochemistry*, **41**, 6376–6382.

Fu, T.-B., Virgilio, L., Narducci, M.G., Facchiano, A., Russo, G. and Croce C.M. (1994) *Cancer Res.*, **54**, 6297.

Fushman, D., Cahill, S., Lemmon, M.A., Schlessinger, J. and Cowburn, D. (1995) *Proc. Natl. Acad. Sci. USA*, **92**, 816–820.

Gibson, T., Hyvönen, M., Musacchio, A., Saraste, M. and Birney, E. (1994) *Trends Biochem. Sci.*, **19**, 349–353.

Guex, N. and Peitsch, M.C. (1997) *Electrophoresis*, **18**, 2714–2723.

Guignard, L., Padilla, A., Mispelter, J., Yang, Y.-S, Stern., M.-H., Lhoste, J.M. and Roumestand C. (2000) *J. Biomol. NMR*, **17**, 215–230.

Haslam, R.J., Koide, H.B. and Hemmings, B.A. (1993) *Nature*, **363**, 309–310.

Hoh, F., Yang, Y.S., Guignard, L., Padilla, A., Stern, M.H., Lhoste, J.M. and van Tilbeurgh, H. (1998) *Structure*, **6**, 147–155.

Ikura, M., Kay, L.E. and Bax, A. (1990) *Biochemistry*, **29**, 4659–4667.

Ishima, R. and Nagayama, K. (1995a) *Biochemistry*, **34**, 3162–3171.

Ishima, R. and Nagayama, K. (1995b) *J. Magn. Reson.*, **B108**, 73–76.

James, S.R., Downes, C.P., Gigg, R., Grove, S.J.A., Holmes, A.B. and Alessi, D.R. (1996) *Biochem. J.*, **315**, 709–713.

Jeener, J., Meier, B.H., Bachman, P. and Ernst, R.R. (1979) *J. Chem. Phys.*, **71**, 4546–4553.

Jones, P.F., Jakubowicz, T., Pitossi, F.J., Maurer, F. and Hemmings, B.A. (1991a) *Proc. Natl. Acad. Sci. USA* **88**, 4171–4175.

Jones, P.F., Jakubowicz, T. and Hemmings, B.A. (1991b) *Cell Regul.*, **2**, 1001–1009.

Kay, L.E., Nicholson, L.K., Delaglio, F., Bax., A. and Torchia, D.A. (1992) *J. Magn. Reson.*, **97**, 359–375.

Koradi, R., Billeter, M. and Wüthrich, K. (1996) *J. Mol. Graph.*, **14**, 51–55.

Künstle, G., Laine, J., Pierron, G., Kagami, S., Nakajima, H., Hoh, F., Roumestand, C., Stern, M.-H. and Noguchi, M. (2002) *Mol. Cell. Biol.* **22**, 1513–1525.

Laine, J., Künstle, G., Obata, Y., Sha, M. and Noguchi, M. (2000) *Mol. Cell.*, **6**, 395–407.

Lander, E.S., Linton, L.M., Birren, B., Nusbaum, C., Zody, M.C., Baldwin, J., Devon, K., Dewar, K., Doyle, M., FitzHugh, W. et al. (2001) *Nature*, **409**, 860–921.

Laskowski, R.A., MacArthur, M.W., Moss, D.S. and Thornton, J.M. (1993) *J. Appl. Cryst.*, **26**, 283–291.

Lefèvre, J.-F., Dayie, K.T., Peng, J.W. and Wagner, G. (1996) *Biochemistry*, **35**, 2674–2686.

Lemmon, M.A. and Ferguson, K.M. (1998) **228**, 39–74.

Lepre, C.A. and Moore, J.M. (1998) *J. Biomol. NMR*, **12**, 493–499.

Lipari, G. and Szabo, A. (1982) *J. Am. Chem. Soc.*, **104**, 4546–4559.

Madani, A., Choukroun, V., Soulier, J., Cacheux, V., Claisse, J.F., Valensi, F., Daliphard, S., Cazin, B., Levy, V., Leblond, V., Daniel, M.T., Sigaux, F. and Stern, M.H. (1996) *Blood*, **87**, 1923–1927.

Madani, A., Soulier, J., Schmid, M., Plichtova, R., Lermé, F., Gateau-Roesch, O., Garnier, J.P., Pla, M., Sigaux, F. and Stern, M.-H. (1995) *Oncogene*, **10**, 2259–2262.

Marion, D., Driscoll, P.C., Kay, L.E., Wingfield, P.T., Bax, A., Gronenborn, A.M. and Clore, G.M. (1989) *Biochemistry*, **28**, 6150–6156.

Mayer, B.J., Ren, R., Clark, K.L. and Baltimore, D. (1993) *Cell*, **73**, 629–630.

Musacchio, A., Gibson, T., Rice, P., Thompson, J. and Saraste, M. (1993) *Trends Biochem. Sci.*, **18**, 343–348.

Nicholson, K.M. and Anderson, N.G. (2002) *Cell. Signal.*, **14**, 381–395.

Nilges, M., Clore, G.M. and Gronenborn, A.M. (1988) *FEBS Lett.*, **229**, 317–324.

Pekarsky, Y., Hallas, C., Isobe, M., Russo, G. and Croce, C.M. (1999) *Proc. Natl. Acad. Sci. USA*, **96**, 2949–2951.

Peng, J.W. and Wagner, G. (1992a) *Biochemistry*, **31**, 8571–8586.

Peng, J.W. and Wagner, G. (1992b) *J. Magn. Reson.*, **98**, 308–332.

Pons, J.L., Malliavin, T.E. and Delsuc, M.A. (1996) *J. Biomol. NMR*, **8**, 445–452.

Press, W.H., Flannery, B.P., Teukolsky, S.A. and Vetterling, W.T. (1986) *Numerical Recipes*, Cambridge University Press, Cambridge.

Rance, M. (1987) *J. Magn. Reson.* **74**, 557–564.

Rebecchi, M.J. and Scarlata, S. (1998) *Annu. Rev. Biophys. Biomol. Struct.*, **27**, 503–528.

Riddles, P.W., Blakeley, R.L. and Zerner, B. (1983) *Meth. Enzymol.*, **91**, 49–60.

Sattler, M., Schleucher, J and Griesinger, C. (1999) *Prog. NMR Spectrosc.*, **34**, 93–158.

Staal, S.P. (1987) *Proc. Natl. Acad. Sci. USA*, **84**, 5034–5037.

Stern, M.H., Soulier, J., Rosenzwajg, M., Nakahara, K., Canki-Klain, N., Aurias, A., Sigaux, F. and Kirsch, I.R. (1993) *Oncogene*, **8**, 2475–2483.

Szewczak, A.A., Kellogg, G.W. and Moore, P.R. (1993) *FEBS Lett.*, **327**, 261–264.

Szyperski, T., Luginbühl, P., Otting, G., Güntert, P. and Wüthrich, K. (1993) *J. Biomol. NMR*, **3**, 151–164.

Thomas, C.C., Deak, M., Alessi, D.R. and van Aalfen, D.M.F. (2002) *Curr. Biol.*, **12**, 1256–1262.

Tjandra, N., Feller, S.E., Pastor, R.W. and Bax, A. (1995) *J. Am. Chem. Soc.*, **117**, 12562–12566.

Tjandra, N., Szabo, A. and Bax, A. (1996) *J. Am. Chem. Soc.*, **118**, 6986–6991.

Yang, J., Cron, P., Good, V.M., Thompson, V., Hemmings, B.A. and Barford, D. (2002) *Nat. Struct. Biol.*, **9**, 940–944.

Yang, Y.-S., Guignard, L., Padilla, A., Hoh, F., Strub, M.P., Stern, M.-H., Lhoste J.M. and Roumestand, C. (1998) *J. Biomol. NMR*, **11**, 339–356.